Electronic signature of DNA bases via Z-shaped graphene nanoribbon with a nanopore

Asma Wasfi[a], Falah Awwad[a,*], Ahmad I. Ayesh[b]

[a] Department of Electrical Engineering, College of Engineering, United Arab Emirates University, P. O. Box 15551, Al Ain, United Arab Emirates
[b] Department of Math., Stat. and Physics, Qatar University, P. O. Box 2713, Doha, Qatar

ABSTRACT

DNA sequencing witnessed significant research efforts to improve its efficiency and to reduce the production cost. Successful DNA sequencing of quick and low cost techniques associate with the personalized medicine as well as procedures and the different genetics subfields of applications. In this article, a novel two-terminal z-shaped sensor is developed and studied to detect the sequence of DNA nucleobases. The z-shaped sensor consists of two metallic zigzag graphene nanoribbon (ZGNR), a semiconducting channel made of armchair graphene nanoribbon (AGNR), and a nanopore in the middle of the channel through which DNA nucleobases are translocated. First-principle modeling and non-equilibrium Green's function along with density functional theory (NEGF + DFT), are utilized to investigate the developed device. Various electronic characteristics are investigated, including transmission spectrum, conductance, and electrical current of DNA nucleobases inside the graphene sensors' nanopore. In particular, these properties are studied with variation of nucleobase orientation. The developed sensor resulted in unique signatures for the individual four DNA nucleobases placed within the nanopore.

1. Introduction

Recent progress in the biomedical field resulted in an increasing need to design inexpensive and efficient DNA sequencing methods. In 1990, the first attempt by Human Genome, was established by the US government with the aim to detect human genome sequence successfully (International Human Genome Sequencing, 2004). In 2003, Human Genome's project was completed successfully with a total cost of $2.7 billion (Hood and Rowen, 2013). During that period of time, Sanger method was utilized to sequence DNA. This method relies on various reagents that are time consuming and costly (Sanger et al., 1977). Due to the high need to understand genes, it is highly critical to develop a low cost method to sequence DNA. Achieving affordable and quick DNA sequencing will offer a map for the entire human genome. This means that people can sequence their genome to find predisposition to diseases, find their weaknesses, and get personalized medicine according to their metabolism. In order to promote the affordability of DNA sequencing, it is estimated that the cost should not exceed $100 per genome cost (International Human Genome Sequencing, 2004). However, more sophisticated sequencing techniques are required to achieve this goal. Methods based on nanopore sequencing (Branton et al., 2008; Venkatesan and Bashir, 2011) and scanning tunneling microscopy (Rajan et al., 2014; Tanaka and Kawai, 2009) provide potential alternatives for the Sanger method (Sanger et al., 1977), especially for detecting single DNA bases by utilizing transverse conductance (Lagerqvist et al., 2006; Zwolak and Di Ventra, 2005). Nanopore sequencing is a main focus of the third-generation sequencing techniques. Biological and solid state nanopores are being utilized (Kim et al., 2019), however solid-state nanopores have become very attractive because they have better stability and easy to control (Wasfi et al., 2018). The main drawback of solid-state nanopores membrane is its thickness which is around 100 times thicker than the distance between two DNA nucleobases. Researchers were motivated to investigate new materials (Liang et al., 2017) such as graphene as it is considered the 21st century magical material. Graphene is a material with two-dimensional arrangement of carbon atoms and extraordinary mechanical and electrical characteristics. Graphene is a unique material since it is highly firm, has a high electrical conductance, high atomic density, high mechanical solidity, and high thermal and electrical conductance. Therefore, graphene is attracting researchers' interests to utilize its unique properties in various applications (Sheka, 2014). Moreover, Graphene oxide (GO) can be utilized as an inexpensive substitute to graphene (Ayesh and Awwad, 2012). Furthermore, hybrid sheet that consists of graphene embedded in hexagonal boron nitride (h-BN)

* Corresponding author.
E-mail address: f_awwad@uaeu.ac.ae (F. Awwad).

provides great potential to distinguish different DNA nucleotides (de Souza et al., 2017). Graphene nanoribbons can be produced by cutting graphene through a method called chirality vector. The two types of graphene nanoribbons (GNRs), based on carbon atoms arrangement and edge termination, are: zigzag (ZGNR) and armchair (AGNR) (Qiu et al., 2014). AGNR behaves like a semiconductor or a metal depending on the number of carbon chains within the width which is denoted by N_a. For $N_a = 3p + 2$, AGNR is metallic, while for $N_a = 3p + 1$ or $N_a = 3p$, it is semiconducting, where p represents a positive integer. Alternatively, ZGNR behaves like a metal (Qiu et al., 2014). The geometry of graphene nanopore affects the DNA sequencing procedure (Zhang et al., 2014). Graphene monolayer thickness is ≈ 0.3 nm; that is similar to the distance between DNA nucleobases, hence, graphene nanopore devices are promising to achieve successful DNA sequencing. Theoretical studies of DNA sequencing through graphene nanopore have proved the possibility of single-base resolution (Al-Dirini et al., 2016; Chang et al., 2014; Comer and Aksimentiev, 2012; Nelson et al., 2010; Prasongkit et al., 2018; Saha et al., 2012; Sarathy et al., 2017). Experimental studies utilizing single or multilayer graphene were preformed (Garaj et al., 2010; Merchant et al., 2010) to measure the vertical ionic current passing through the DNA bases. A number of experimental (Huang et al., 2010; Tsutsui et al., 2010) and theoretical proposals (Chen et al., 2012; Zwolak and Di Ventra, 2007) adapted the transverse current approach which relied on first-principle approaches to analyze the tunneling current for DNA bases translocating through a nanogap between two metallic electrode of ZGNR structure (He et al., 2011; Prasongkit et al., 2011), or through a nanopore within AGNR semiconducting armchair graphene nanoribbons (Nelson et al., 2010).

Numerous nanotechnology based sensors have been fabricated and studied for DNA sequencing since they are amplification free, label free, and can be improved to acquire high throughput analysis. Various techniques employed graphene, which include the passage of DNA through graphene nanogaps, nanopores, nanoribbons, and the DNA physisorption on graphene membranes (Heerema and Dekker, 2016). The key techniques for DNA sequencing using graphene nanostructures are: (i) Ionic current identification through a pore in graphene membrane where a graphene membrane with a nanopore is placed in an electrolytic solution. DNA strand passes through the pore because of the electric field. As the DNA bases pass through the pore, it blocks the ionic current applied to the membrane. Each base results in a unique current blockage due to the nucleobase shape and size. (ii) DNA sequencing using tunneling through graphene nanogap. The idea here is to measure the conductance of the bases passing through two graphene electrodes. A unique tunneling conductance will result for each of the bases. In this approach, graphene represent both the electrodes and the membrane making the sensor fabrication process easy. (iii) DNA detection due to current differences through graphene nanoribbon where nanostructured graphene is utilized to detect the sequence by measuring the current of DNA bases passing through a pore in a graphene nanoribbon. Zigzag and armchair graphene nanoribbons provide promising results for DNA detection. (iv) DNA bases physisorption onto graphene membrane results in current change. The DNA bases' interaction with graphene membrane results in current variations and various interaction strengths. Graphene nanopore offers a proper technique for single and double stranded DNA detection because of its scalable production, cost, and process speed. Noise is one of the main issues of graphene based sensors however noise can be lowered by employing multilayered graphene and by reducing the freestanding graphene (Garaj et al., 2013). Also, DNA adsorption approach reduces the noise levels (Heerema and Dekker, 2016). Graphene nanoribbon approach allows higher bandwidths measurements which will enable measuring the sequence at higher speed (Heerema and Dekker, 2016).

Nowadays, it is becoming substantially important to study single atom effect in device simulations since the electronic devices feature size is emulating the atomic scale. Various simulators were developed using non-equilibrium Green's function (NEGF) (Haug and Jauho,

2008). Molecular simulations have a great importance in the nanopore research field (Kim and Kim, 2015). These simulations are utilized to interpret the actual results (Aksimentiev, 2010). The techniques can be categorized into two groups: semi-empirical techniques which include methods based on extended Hückel and SlaterKoster tight-binding, and ab-initio techniques which are found on the density functional theory (Stokbro et al., 2010). Semi-empirical computational methods' cost is less than the ab-initio methods. However, ab initio methods (computational methods that describe the properties of materials based on basic laws without previous knowledge or assumptions) provide more predictive power and reasonable results without prior experimental data. In this article, our device is studied using the first-principle modeling non-equilibrium Green's function along with density functional theory (NEGF + DFT). Furthermore, simulation of electronic transport is conducted by employing first-principle calculations utilizing NEGF + DFT. The atomistic structure of the z-shaped sensor is displayed, and the computational method utilized to optimize the device and calculate the various electronic properties are illustrated. Moreover, the device's zero bias transmission spectrum for each nucleobase within the graphene nanopore at different orientations, the conductance, and the electrical current at 0.5 V bias voltage at room temperature are discussed.

2. Z-shaped sensor configuration

Fig. 1 represents the nanoscale device setup introduced in this work. The z-shaped metal-semiconductor-metal junction device consists of the following regions: the electrodes (right and left) and the main central region. The left and right electrodes consist of metallic zigzag graphene nanoribbons while the middle is made of armchair graphene nanoribbon with a width of 13 carbon chains which makes the AGNR semiconducting. A nanopore of size 10.1 Å is created in the central region. The nanopore carbon atoms of the edge and graphene nanoribbons are passivated with hydrogen. This study evaluates the performance of the graphene nanopore that is utilized for DNA sequencing, by employing first-principles calculations using Quantumwise (ATK-VNL) package. First-principles ATK-VNL simulation which is built on non-equilibrium NEGF + DFT are used to investigate the transmission spectrum, conductance, and current of DNA nucleobases inside the graphene nanopore. All these characteristics are studied with variation in nucleobase orientation. DNA backbones of sugar and phosphate groups are not considered in the simulation. The backbone contribution is ignored, as the background noise coming from the backbone may be determined and subtracted from the signal of individual nucleobases (Ahmed et al.,
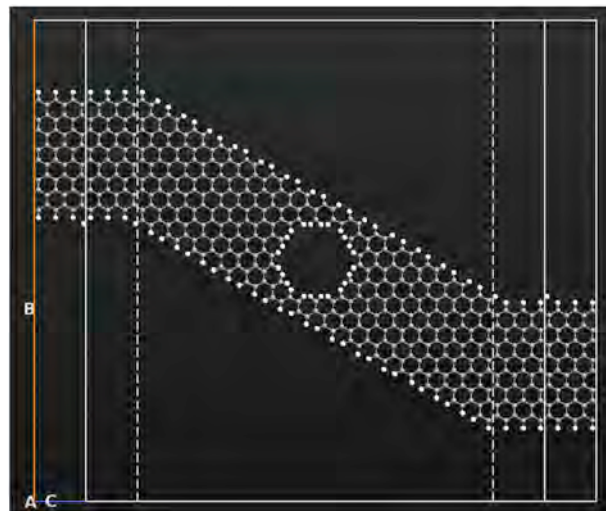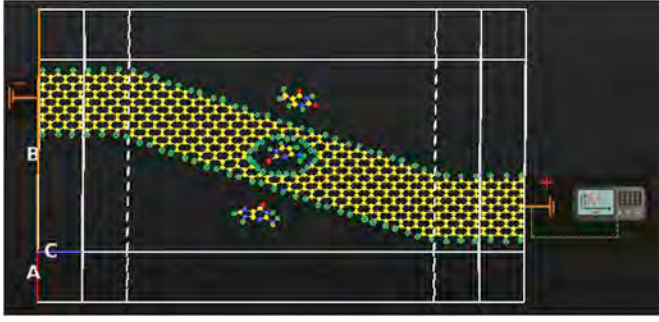

Fig. 1. Schematic view of z-shaped DNA sensor.

Fig. 2. Schematic representation of z-shaped graphene nanoribbon with nanopore where isolated DNA bases move inside the nanopores and transverse electronic current flow through the membrane. The edge carbon atoms of the nanopore and of the graphene nanoribbon are passivated by hydrogen. (Carbon-yellow, Hydrogen-green, Nitrogen-blue, Oxygen-red).

2014).

2.1. Z-shaped sensor structure

Fig. 2 shows the z-shaped sensor hosting a nanopore of 10.1 Å diameter where DNA bases translocate. The current flow is perpendicular to the DNA bases. The width of the armchair graphene nanoribbon and the nanopore is fixed. Armchair width is 16.61 Å, while the nanopore size is 10.1 Å. Finite bias voltage is applied between left and right electrode which is fixed as $+0.25$ and -0.25 V.

Because of the different chemical and electronic structure of the four nucleobases, each one of them has a unique signature. Our main objective in this study is to find the relative current for each nucleotide where we seek to find a unique electronic signature for each base to create a DNA electronic map. In this article, we study the effect of the electronic and chemical structure of the DNA bases in charge transport.

3. Computational methods

Prior to ATK-VNL transport calculations, the density functional theory is utilized to optimize the device and nucleobases and to relax all atoms until the individual atomic force is below 0.05 eV/Å. All optimizations are completed by the density functional theory. The Perdew-Burke-Ernzerhof parametrization for the generalized gradient approximation (GGA) is utilized for the exchange and correlation function (P. Perdew et al., 1996). The employed density mesh cut-value of energies is 400 eV. A $1 \times 1 \times 1$ k-point mesh is utilized for the Brillouin zone integration within Monkorst-Pack scheme. The density functional theory is used to describe our device, where an extension of this method is the formalism of NEGF which is used to describe the quantum transport phenomena. The NEGF formalism sets the concept to study the electronic transport at quantum level to calculate the desired quantities such as conductance and current for the DNA sensor.

Density functional theory along with local density approximation (LDA) limits and Perdew Zungar exchange correlation function (Perdew et al., 1981) impeded in the ATK-VNL simulation package are employed. The ZGNR and AGNR of the left and right electrodes are classified by the ribbon width. A mesh cut-off of 65 Hartree is fixed to display the charge density. A grid of $2 \times 2 \times 100$ k-points is utilized to perform the sampling of the Brilloin Zone integration. The transmission spectrum as a function of bias, conductance, and current are determined by utilizing the NEGF as integrated in the ATK-VNL.

The zero bias transmission spectrum between the source and drain is calculated as (Chang et al., 2014; Saha et al., 2012):

$$T(E) = Tr\{\Gamma_D(E)G(E)\Gamma_S(E)G^\dagger(E)\} \tag{1}$$

where, E is the energy, Tr is the trace, $\Gamma_{D,\,S}(E) = i[\sum_{L,\,R}(E) - \sum_{S,\,D}^\dagger(E)]$ describes the broadening level because of the coupling to the electrodes,

i refers to iteration, and $\sum_{L,\,R}(E)$, $\sum_{S,\,D}^\dagger(E)$ are the self-energies presented by the electrodes.

The linear response conductance at a certain temperature (T) is determined from the transmission function by the standard Landauer formula for devices with two terminals (Chang et al., 2014; Saha et al., 2012):

$$G(E_F) = \frac{2e^2}{h} \int_{-\infty}^{\infty} dE\ T\left(-\frac{\partial f}{\partial E}\right) \tag{2}$$

where, $G_0 = \frac{2e^2}{h}$ is the conductance quantum which is $\approx 7.7480917310 \times 10^{-5}$ S, $f(E) = \{1 + \exp[(E - \mu)/k_BT]\}^{-1}$ is defined as the Fermi function of some macroscopic reservoirs where semi-infinite ideal contact leads terminate, $\mu = E_F$ refers to the electrode chemical potential, and k_B is Boltzmann's constant.

The electron transmission spectrum as a function of bias is evaluated utilizing NEGF method, as integrated in ATK-VNL, using (Chang et al., 2014):

$$T(E, V_b) = Tr\{\Gamma_D(E, V_D)G(E)\Gamma_S(E, V_S)G^\dagger(E)\} \tag{3}$$

where, G and $G^\dagger$ are associated with advanced Green's function of the main scattering region, and where V_b is the bias voltage between source (V_s) and drain (V_d). S, D, L, and R refer to the source, drain, left, and right. The transmission spectrum function T(E,V) illustrates the probability for quantum mechanical transmission of electrons. The right and left electrodes' semi-infinite effect is considered by creating the self-energies $\sum_{L,\,R}(E)$ and $\sum_{S,\,D}^\dagger(E)$ in the effective Hamiltonian.

The integration of T(E, V) over the energy window determined using the difference of the Fermi functions $f_{S,\,D}(E) = \{1 + \exp[(E - E_F - eV_{S,D})/k_BT]\}^{-1}$ gives the total current (Chang et al., 2014):

$$I = \frac{2e}{h} \int_{-\infty}^{\infty} dE\ T(E, V)[f_S(E) - f_D(E)] \tag{4}$$

4. Results and discussion

4.1. Transmission spectrum

The developed sensor transmission spectrum is calculated by ATK-DFT calculator using Troullier-Martins norm-conserving pseudopotentials, local density approximation with Perdew-Zungar (PZ) parametrization chosen for the exchange correlation function of DFT, and the pseudoatomic local orbitals for carbon and hydrogen atoms which are single zeta polarized. The mesh within Mokhorst-Pack scheme in the Brillouin zone integration is $2 \times 2 \times 100$ k-point. The sampling points in the energy range -2 to 2 eV are 200. The transmission spectrum of the device with 1.1 Å nanopore without any applied bias potential is shown in Fig. 3 The transmission spectrum reflects the central semiconducting AGNR electronic structure. The low transmission in the -1 to 0.3 eV energy range is due to the band gap region of the central device. Due to the absence of energy levels within this region, the electrons should tunnel to pass through the junction.

Various orientations of the nucleobases occur through the graphene nanopore during the translocation of a single stranded of DNA. Therefore, it is highly important to study the effect of nucleobase orientation on the transmission spectrum. The transmission spectrum at zero bias of the nanoscale sensor is computed for each nucleobase with various rotations. Each base is rotated 180° around x-axis, 180° around xy-plane, and 180° around xz-plane. The zero bias transmission spectrum is affected by the various types of base orientations. The nucleobases are divided into two groups: purine bases that contain Adenine and Guanine, and pyrimidine bases that contain Cytosine and Thymine. The base size is the main distinctive feature between purine and pyrimidine bases.
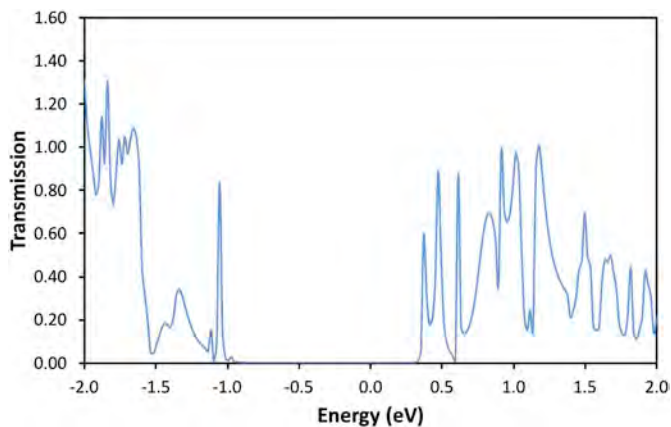
Fig. 3. The zero bias transmission spectrum for z-shaped device with a nanopore in the middle.

The rotation effect of the nucleobases (Adenine, Guanine, Cytosine, and Thymine) on the transmission spectrum is shown in Fig. 4. Each nucleobase is rotated from 0 to 180 around the x-axis, xy-plane, and xz-plane. For example, the four types of nucleobases orientations corresponding to 0° are shown in Fig. 5.

4.2. Conductance

Fig. 6 is produced using NEGF + DFT simulations. Fig. 6 (a) shows the conductance resulting from various orientation of nucleobases presented in Fig. 7. Fig. 6 (b) shows the integration of the conductance

with different orientations for each nucleobase inserted in the nanopore at room temperature (300 K). The conductance at room temperature is calculated from transmission spectra using equation (2). Fig. 6 reveals that purine base (Adenine and Guanine) have less conductance than pyrimidine bases (Cytosine and Thymine) due to the physical and chemical structures of these bases which make it possible to identify the two groups of DNA nucleobases at an applied bias voltage.

A critical issue is to study the signal modification when DNA bases orientation vary inside the nanopore. For selected orientation of DNA bases shown in Fig. 7(a–d), the conductance variations are displayed in Fig. 6. The intervals in Fig. 6 (b) are the limits of conductance change because not all values inside the interval can be sampled experimentally. Some of the bases orientations in Fig. 7 are chosen to get maximum conductance change and they involve specific bending of DNA bases to place the base into such position.

Our study illustrate that each DNA nucleobase will lead to a significant charge density modulation and to significant related electronic potential in the surrounding area.

4.3. Current

The electrical current is also measured since it is detected in experimental work. Fig. 8 shows the electrical current variation because of nucleotide rotation. Thymine and Cytosine have higher current ranges than Adenine and Guanine which makes it easier to distinguish purine and pyrimidine bases. The current passing through each base, gives a unique signature as displayed in Fig. 8. These electrical signatures differ for the various orientations of the bases.

The main idea is that when DNA strands go across the nanopore, the current passing through the graphene nanopore will be unique for each
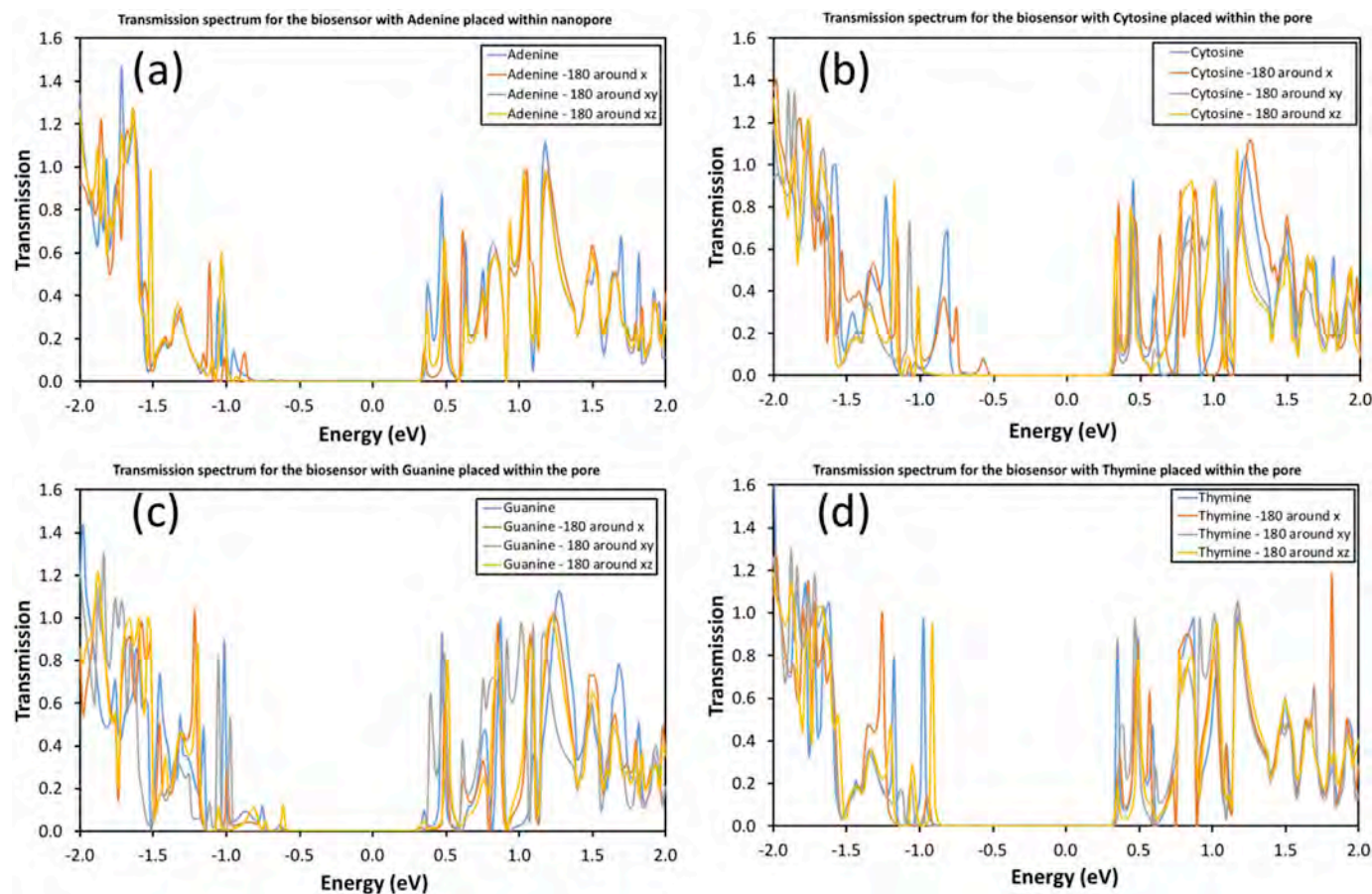

Fig. 4. The zero bias transmission spectra for the four nucleobases: (a) Adenine, (b) Guanine, (c) Cytosine, and (d) Thymine. The transmission curves respective colors indicate the nucleobase orientation within the pore.
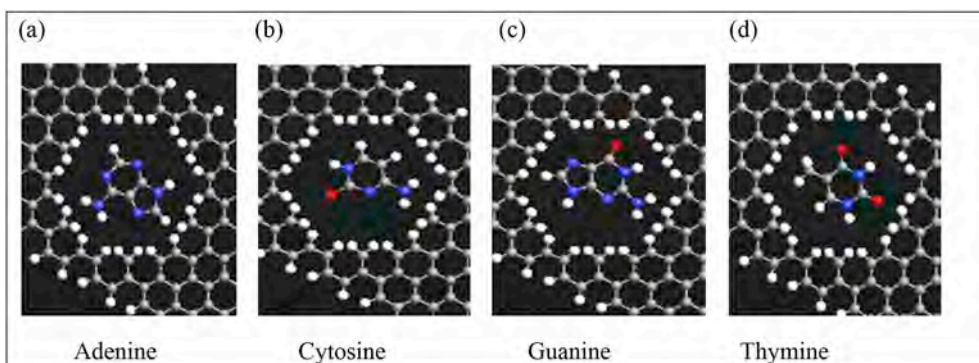
Fig. 5. The four types of nucleobases orientations corresponding to 0°: (a) Adenin, (b) Guanine, (c) Cytosine, and (d) Thymine.

base A, C, G, and T. The current passing through the nanopore is influenced by the electrostatic interaction among the pore and the bases which results in a difference in the local density of states in the graphene membrane around the pore. Placing a DNA base in graphene nanopore influences the charge density within the surrounding area. This leads to a distinctive current for each nucleobase. The current is measured from the integrated density of state. The DNA bases' translocation through the nanopore leads to different orientation of the nucleobases which will affect the current.

Finite bias voltage is applied between the source and drain $V_b = V_s - V_d$. The various spatial extension of the nucleobases affect their influence to the density of states where the density of states is used to calculate current and conductance. These variations in the spatial extension are influenced by the nucleobase orientation and geometry.

Pyrimidine and purine will have differences in their electronic states and spatial extension which will result in a difference in the density of states for the nucleobases placed within the nanopore. DNA is made up of diverse bases connected to sugar phosphate backbone. The four bases that build up polymers are categorized into two groups: the pyrimidine bases C and T and the purine bases A and G. The pyrimidines bases comprise of six membered ring while the purine bases comprise of a six and a five membered ring. This classification is based on the chemical structure. Since purines are larger, they would have stronger interaction in a confined space. This causes reduced separation but stronger coupling of G and A with the nanopore compared with C and T.

5. Comparative analysis

Intensive studies have been performed on transverse current of various electrode-nucleotide coupling (Krems et al., 2009; Lagerqvist et al., 2007; Meunier and Krstic, 2008). However, most of these studies faced the issue of interference between adjacent nucleobases since DNA bases length is ≈ 0.32 nm which is much smaller than the thickness of most electrodes' material such as gold. This makes it difficult to
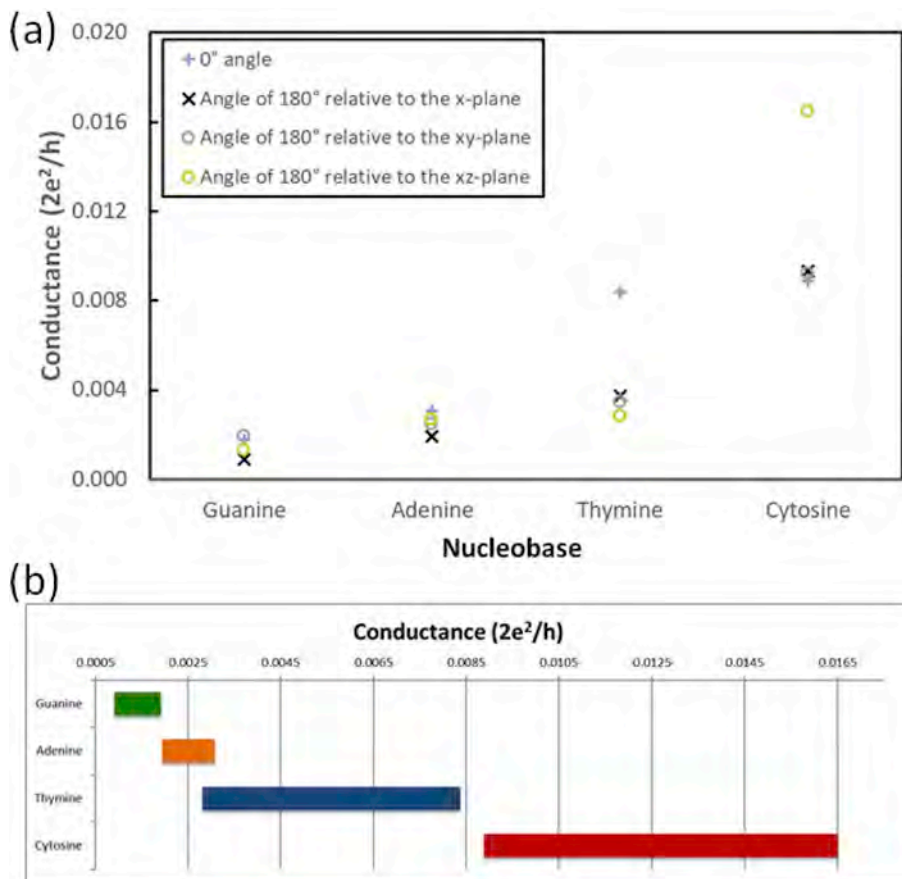

Fig. 6. (a) The room temperature conductance for the z-shaped sensor for each nucleobase inserted within the pore due to rotations. The conductance is calculated using quantum simulations by employing first principles model. (b) The room temperature conductance intervals due to change of the spatial orientations of nucleobases with respect to the pore.
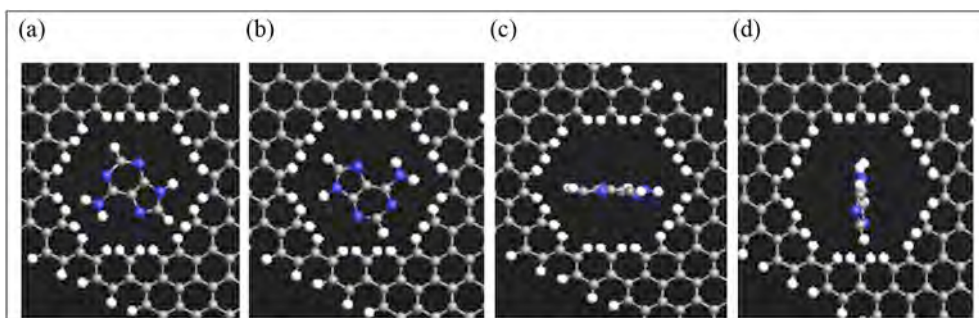
Fig. 7. (a) Adenine placed within the nanopore at 0° angle. (b) Adenine at an angle of 180° relative to the x-plane. (c) Adenine at an angle of 180° relative to the xy-plane. (d) Adenine at an angle of 180° relative to the xz-plane.

differentiate the neighboring bases (He et al., 2010; Lagerqvist et al., 2006). An alternative technique is the transverse electronic based sensors with a nanogap (Postma, 2010). The present sensor is based on graphene, which is one atom thick, where the nanopore thickness is similar to the DNA nucleobases dimensions. Moreover, single and multilayer graphene experiments based on measuring the vertical ionic current of passing DNA, didn't provide adequate resolution to identify the different nucleobases (Branton et al., 2008; Healy et al., 2008) Various experimental (Huang et al., 2010; Tsutsui et al., 2010) and theoretical (Chen et al., 2012; Zwolak and Di Ventra, 2007) studies on nanogaps were conducted, but resulted in very small current of picoampere (Prasongkit et al., 2011). First-principle studies based on two metallic graphene nanoribbon hosting a nanogap resulted in current variations for the different nucleobases inside the gap, a major drawback was the low conductance (He et al., 2011). Moreover, a nanogap may permit several DNA bases to translocate through the gap

simultaneously resulting in signal interference problem. As nanopore has low dimension size in contrast with a nanogap, thus, our developed sensor did avoid the simultaneous DNA sequence issue. Moreover, the results in (McFarland et al., 2015) showed that at 0.5 V purine bases (Adenin and Guanine) have less current than pyrimidine bases (Cytosine and Thymine) which is consistent with our work. On the other hand, at 1 V purine bases have more current than pyrimidine bases (Lagerqvist et al., 2006; Prasongkit et al., 2011).

Since the four nucleobases exhibit different chemical and electronic structure, each one of them has a unique signature. Our main objective in this study is to determine the relative current for each nucleotide where we seek to find a unique electronic signature for each base to create a DNA electronic map. We studied the effect of the electronic and chemical structure of the DNA bases in charge transport. Also, it was found that the nuleotides' orientations affect the electronic signature. Our sensor was able to discriminate the four bases by providing a
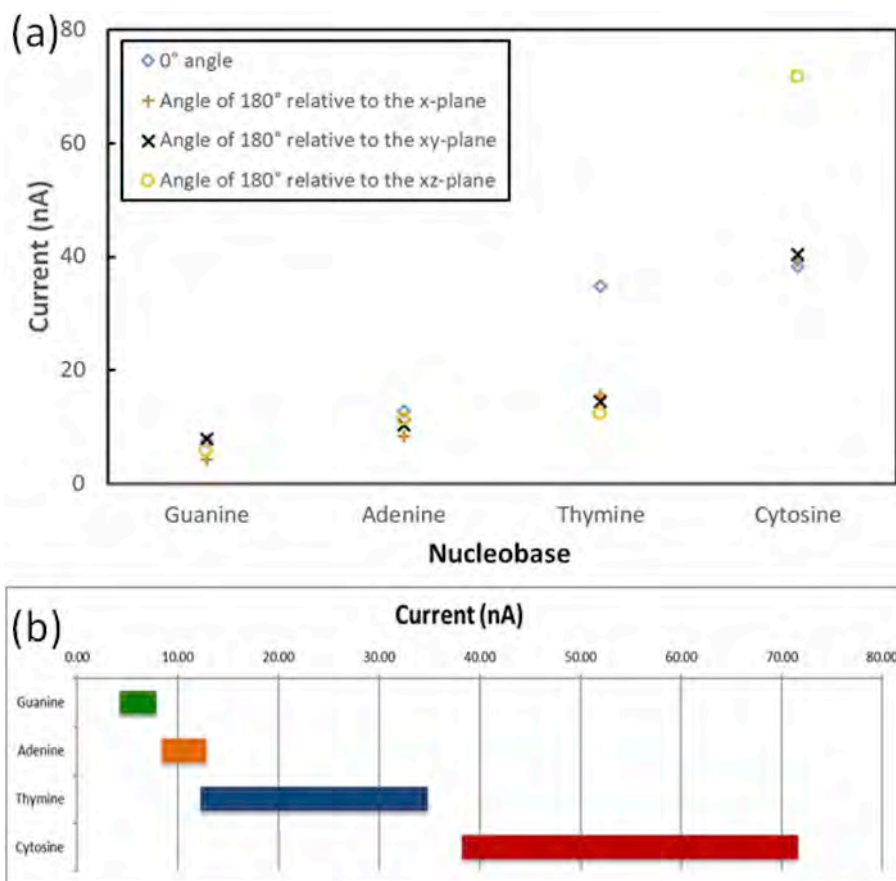

Fig. 8. (a) Current variation due to nucleotide rotation in the z-shaped sensor pore at 0.5 V bias; (b) Current intervals due to nucleotide rotation at 0.5 V bias.

unique current and conductance range for each base. Our study suggests that our graphene bases sensor promise successful and fast method for DNA sequencing. It delivers great motivation for the advance of novel class devices for nanopore sequencing.

6. Conclusion

In summary, a two terminal z-shaped nanostructured sensor that consists of two metallic electrodes connected through a semiconducting channel with a nanopore in the middle is investigated in this work. The four DNA nucleobases are inserted in a hydrogen passivated nanopore, leading to unique differences in the device transmission spectrum, current, and conductance. First-principle transport simulations are conducted for a novel nanopore graphene based sensor to achieve an accurate DNA sequencing. The results show that each base generates a unique signature of conductance and current at 0.5 bias voltage. The main nucleobases: Adenine, Thymine, Cytosine, and Guanine interactions with the graphene nanopore results indicate that the sensor conductance and current are sufficiently sensitive to distinguish the different nucleobases. Moreover, it is found that the nucleobase orientation within the nanopore affect the current and conductance.

Our work suggests that nanopore based graphene sensor provides a robust technology for DNA sequencing and gives a strong motivation for new nanopore sequencing devices development. It reveals a unique electronic signature for each of the four nucleobases which provides us with DNA electronic map. The presented sensor expounds potential to develop accurate, fast, and affordable technique for next generation DNA sequencing and detection.

Declaration of interests

- The authors declare that they have no known competing financial interests or personal relationships that could have appeared to influence the work reported in this paper.
- The authors declare the following financial interests/personal relationships which may be considered as potential competing interests:

Note

The authors declare no competing financial interest.

CRediT authorship contribution statement

Asma Wasfi: Software, Validation, Formal analysis, Investigation, Writing - original draft, Writing - review & editing, Visualization. **Falah Awwad:** Conceptualization, Methodology, Investigation, Resources, Writing - original draft, Writing - review & editing, Supervision, Project administration, Funding acquisition. **Ahmad I. Ayesh:** Conceptualization, Methodology, Investigation, Resources, Writing - original draft, Writing - review & editing.

Acknowledgment

References

Ahmed, T., Haraldsen, J.T., Rehr, J.J., Di Ventra, M., Schuller, I., Balatsky, A.V., 2014. Nanotechnology 25 (12), 125705.

Aksimentiev, A., 2010. Nanoscale 2 (4), 468–483.

Al-Dirini, F., Mohammed, M.A., Hossain, M.S., Hossain, F.M., Nirmalathas, A., Skafidas, E., 2016. Nanoscale 8 (19), 10066–10077.

Ayesh, A.I., Awwad, F., 2012. J. Nanomater. Mol. Nanotechnol. 1 (1) 2324-8777.

Branton, D., Deamer, D.W., Marziali, A., Bayley, H., Benner, S.A., Butler, T., Di Ventra, M., Garaj, S., Hibbs, A., Huang, X., Jovanovich, S.B., Krstic, P.S., Lindsay, S., Ling, X.S., Mastrangelo, C.H., Meller, A., Oliver, J.S., Pershin, Y.V., Ramsey, J.M., Riehn, R., Soni, G.V., Tabard-Cossa, V., Wanunu, M., Wiggin, M., Schloss, J.A., 2008. Nat. Biotechnol. 26 (10), 1146–1153.

Chang, P.-H., Liu, H.K., Nikolic, B., 2014. J. Comput. Electron. 13 (4), 847–856.

Chen, X., Rungger, I., Pemmaraju, C.D., Schwingenschlögl, U., Sanvito, S., 2012. Phys. Rev. B 85 (11), 115436.

Comer, J., Aksimentiev, A., 2012. Nanomater. Interfaces 116 (5), 3376–3393.

de Souza, F.A., Amorim, R.G., Scopel, W.L., Scheicher, R.H., 2017. Nanoscale 9 (6), 2207–2212.

Garaj, S., Hubbard, W., Reina, A., Kong, J., Branton, D., Golovchenko, J.A., 2010. Nature 467 (7312), 190–193.

Garaj, S., Liu, S., A Golovchenko, J., Branton, D., 2013. Proc. Natl. Acad. Sci. U. S. A 110 (30), 12192–12196.

Haug, H., Jauho, A.-P., 2008. Quantum Kinetics in Transport & Optics of Semiconductors.

He, Y., Shao, L., Scheicher, R., Grigoriev, A., Ahuja, R., Long, S., Ji, Z., Zhaoan, Y., Liu, M., 2010. Appl. Phys. Lett. 97 (4), 043701.

He, Y., Scheicher, R., Grigoriev, A., Ahuja, R., Long, S., Huo, Z., Liu, M., 2011. Advanced Functional Materials. pp. 2674–2679.

Healy, K., Schiedt, B., Morrison, A., 2008. Nanomedicine 875–897.

Heerema, S.J., Dekker, C., 2016. Nat. Nanotechnol. 11 (2), 127–136.

Hood, L., Rowen, L., 2013. Genome Med. 79 (5).

Huang, S., He, J., Chang, S., Zhang, P., Liang, F., Li, S., Tuchband, M., Fuhrmann, A., Ros, R., Lindsay, S., 2010. Nat. Nanotechnol. 5 (12), 868–873.

International Human Genome Sequencing, C., 2004. Nature 431, 931.

Kim, H.S., Kim, Y.H., 2015. Biosens. Bioelectron. 69, 186–198.

Kim, H.J., Choi, U.J., Kim, H., Lee, K., Park, K.B., Kim, H.M., Kwak, D.K., Chi, S.W., Lee, J.S., Kim, K.B., 2019. Nanoscale 11 (2), 444–453.

Krems, M., Zwolak, M., Pershin, Y.V., Di Ventra, M., 2009. Biophys. J. 97 (7), 1990–1996.

Lagerqvist, J., Zwolak, M., Di Ventra, M., 2006. Nano Lett. 6 (4), 779–782.

Lagerqvist, J., Zwolak, M., Di Ventra, M., 2007. Biophys. J. 93 (7), 2384–2390.

Liang, L., Shen, J.W., Zhang, Z., Wang, Q., 2017. Biosens. Bioelectron. 89 (Pt 1), 280–292.

McFarland, H.L., Ahmed, T., Zhu, J.X., Balatsky, A.V., Haraldsen, J.T., 2015. J. Phys. Chem. Lett. 6 (13), 2616–2621.

Merchant, C.A., Healy, K., Wanunu, M., Ray, V., Peterman, N., Bartel, J., Fischbein, M.D., Venta, K., Luo, Z., Johnson, A.T., Drndic, M., 2010. Nano Lett. 10 (8), 2915–2921.

Meunier, V., Krstic, P.S., 2008. J. Chem. Phys. 128 (4), 041103.

Nelson, T., Zhang, B., Prezhdo, O.V., 2010. Nano Lett. 10 (9), 3237–3242.

Perdew, P., Zunger, J.A., 1981. Phys. Rev. B 5048–5079.

Perdew, P., Burke, J.K., Ernzerhof, M., 1996. Phys. Rev. Lett. 3865–3868.

Postma, H.W., 2010. Nano Lett. 10 (2), 420–425.

Prasongkit, J., Grigoriev, A., Pathak, B., Ahuja, R., Scheicher, R.H., 2011. Nano Lett. 11 (5), 1941–1945.

Prasongkit, J., de Freitas Martins, E., de Souza, F.A.L., Scopel, W.L., Amorim, R.G., Amornkitbamrung, V., Rocha, A.R., Scheicher, R.H., 2018. J. Phys. Chem. C 122 (13), 7094–7099.

Qiu, W., Nguyen, P., Skafidas, E., 2014. Phys. Chem. Chem. Phys. : Phys. Chem. Chem. Phys. 16 (4), 1451–1459.

Rajan, A.C., Rezapour, M.R., Yun, J., Cho, Y., Cho, W.J., Min, S.K., Lee, G., Kim, K.S., 2014. ACS Nano 8 (2), 1827–1833.

Saha, K.K., Drndic, M., Nikolic, B.K., 2012. Nano Lett. 12 (1), 50–55.

Sanger, F., Nicklen, S., Coulson, A.R., 1977. Proc. Natl. Acad. Sci. Unit. States Am. 74 (12), 5463–5467.

Sarathy, A., Qiu, H., Leburton, J.-P., 2017. J. Phys. Chem. B 121 (15), 3757–3763.

Sheka, E., 2014. Int. J. Quantum Chem. 114 (16).

Stokbro, K., Petersen, D., Smidstrup, S., Blom, A., Ipsen, M., Kaasbjerg, K., 2010. Phys. Rev. B 82, 075420.

Tanaka, H., Kawai, T., 2009. Nat. Nanotechnol. 4 (8), 518–522.

Tsutsui, M., Taniguchi, M., Yokota, K., Kawai, T., 2010. Nat. Nanotechnol. 5 (4), 286–290.

Venkatesan, B.M., Bashir, R., 2011. Nat. Nanotechnol. 6 (10), 615–624.

Wasfi, A., Awwad, F., Ayesh, A.I., 2018. Biosens. Bioelectron. 119, 191–203.

Zhang, Z., Shen, J., Wang, H., Wang, Q., Zhang, J., Liang, L., Agren, H., Tu, Y., 2014. J. Phys. Chem. Lett. 5 (9), 1602–1607.

Zwolak, M., Di Ventra, M., 2005. Nano Lett. 5 (3), 421–424.

Zwolak, M., Di Ventra, M., 2007. Rev. Mod. Phys. 80 (1), 141–165.